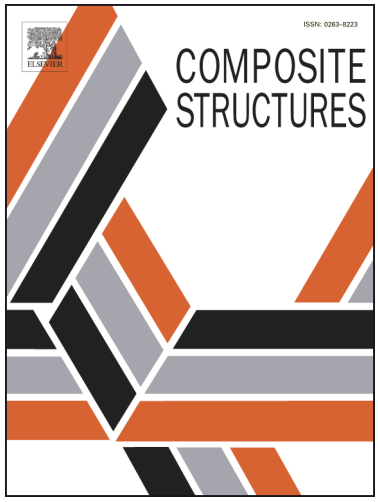


# Tensile and fatigue properties of single lap joints of aluminium alloy/glass fibre reinforced composites fabricated with different joining methods

M. Mariam, M. Afendi, M.S. Abdul Majid, M.J.M. Ridzuan, A.G. Gibson

PII: S0263-8223(18)31561-7
DOI: https://doi.org/10.1016/j.compstruct.2018.06.003
Reference: COST 9797

To appear in: *Composite Structures*

Received Date: 27 April 2018
Accepted Date: 1 June 2018

Please cite this article as: Mariam, M., Afendi, M., Majid, M.S.A., Ridzuan, M.J.M., Gibson, A.G., Tensile and fatigue properties of single lap joints of aluminium alloy/glass fibre reinforced composites fabricated with different joining methods, *Composite Structures* (2018), doi: https://doi.org/10.1016/j.compstruct.2018.06.003

# Tensile and fatigue properties of single lap joints of aluminium alloy/glass fibre reinforced composites fabricated with different joining methods

M. Mariam[a], M. Afendi[a*], M.S. Abdul Majid[a], M.J.M. Ridzuan[a], A.G. Gibson[b]

[a] *School of Mechatronic Engineering, Universiti Malaysia Perlis, Pauh Putra Campus, 02600 Arau, Perlis, Malaysia,*
[b] *School of Mechanical and Systems Engineering, Newcastle University, Newcastle upon Tyne, NE1 7RU, UK*

*Author email addresses:mariam.bt.majid@gmail.com, *afendirojan@unimap.edu.my, shukry@unimap.edu.my, ridzuanjamir@unimap.edu.my, geoff.gibson@newcastle.ac.uk*

** Corresponding author*

## Abstract

The tensile and fatigue properties of single similar and dissimilar lap joints of aluminium alloy (AA7075) and glass fibre reinforced epoxy (GRE) composite were investigated. Three joining methods were employed: mechanically fastened Huck bolted joints, Araldite epoxy adhesive bonded joints and hybrid joints comprising adhesive and Huck bolts. Tensile-shear fatigue tests were performed using single lap joint specimens at the stress ratio R=0.1 to determine the fatigue behaviour of the joints. Subsequently, S–N curves were drawn for different levels of stress amplitude (30%, 40%, 50%, 60%, 70%, 80% and 90%). The micro structures of the fractured surfaces were examined by field emission scanning electron microscopy. The experimental results show that the hybrid joints with dissimilar adherends exhibit the highest strength and stiffness, with predominantly mix-mode failure and shear-out tension of the Huck bolt. These two failure mechanisms were detected as primary and secondary failures in the hybrid joint.

**Keywords**:

Fatigue; glass fibre-reinforced epoxy (GRE); Huck bolt;

## 1. Introduction

Over the years, modern aerospace and automotive manufacturers have continually strived to reduce weight, aiming for high-stiffness structures involving metallic and composite materials. Lightweight structural parts are attractive for use in design and manufacturing in automotive industries as they can provide 20-30% reduction in the total weight [1]. In order to improve fuel economy and reduce environmental emissions, the materials used in the transportation industries are changing from mostly low-carbon steels to a combination of advanced high-strength steels and lightweight alloys. This includes the use of aluminium alloys, magnesium alloys and polymer matrix composites, which are providing an efficient means to reduce vehicle mass. Even though the aluminium alloy has substantially lower strength and stiffness than steels, it is successfully compensated in the design of a car spaceframe, where a thicker material produced a smooth joining. In automotive industry applications, various joining processes have been introduced, such as friction lap welding [2], laser-assisted direct joining [3,4], friction riveting, and flow drilling. To satisfy the various requirements of the automotive and aerospace industries, the combination of dissimilar adherends has been introduced, particularly for joining non-metals to metals, as applied in research. The mechanical properties and joining techniques of adherends are an essential factor in structural applications.

For the past few decades, the joining techniques used were adhesive bonding, bolt fastening, and adhesive-bolt hybrid joining; this has led to various researches studies on the combination of dissimilar materials and the joining methods [5]: single-lap [6], double-lap [7-9], scarf [10,11], strapped [12,13], and tapered joints [6]. The mechanical fastening methods riveting, screw-type fasteners, washers and bolt and nut were used in the bolting condition and always required drill holes on the substrates. This is typically more efficient in metallic substrates than in composites as they are more ductile. However, drilled holes on bolted joints introduce stress concentrations, resulting in a tendency to form cracks that can grow and cause failure. According to Pinto et al. [14], the effects of stress concentration and large deformation as a result of drilling holes never benefit the joint strength, as the joint efficiency and quality depend on machined holes. Thus, the high stress concentration was found to be more severe in composite laminates than in metal plates [15]. Adhesively bonded joint is a process requiring two or more solid parts known as substrates/adherends with an adhesive substance in between. The performance and durability of adhesive have enhanced significantly with the advancements of polymer science. Moreover, this type of bonding has many advantages over

the more conventional joining methods of fusion and spot welding, bolting, and riveting, as it can bond dissimilar materials, resulting in high stiffness, better fatigue performance, and uniform stress distribution over a large bond area [16-17]. Previously, adhesive bonding is mostly part-utilised for auxiliary structures when the failure does not directly affect the structural safety due to the high specific stiffness and strength, low cost, smooth configuration, and uniform stress distribution associated with the joining method [5]. In automotive space frames, the time consumed in the joining production process is most important and is the main concern that contributes to the disadvantages of an adhesively bonded joint. In addition, there may be difficulties in separating the adhesive bonds that need regular maintenance service and repair [18]. However, past studies have shown that the stress concentration of an adhesively bonded joint is lesser than that in a bolted joint.

In order to enhance the joining performance, both bolted and adhesive bonded joints were combined to develop a joining mechanism with improved mechanical behaviour. In recent decades, this combined application has gained more attention in modern aerospace and automotive industries owing to its greater performance. This combination is known as a hybrid joint. A hybrid joint offers several advantages in automotive production over other methods in terms of process ability and load bearing capacity: greater strength, stiffness and fatigue life [19-21]. Numerous experimental studies have shown that such hybrid joints can potentially achieve higher static strength than the underlying bonded and bolted joints could separately [5, 22, 23]. The hybrid single lap joint was experimentally applied in the static and fatigue loading of composite materials by Fu and Mallick [21]. The study showed that higher static loading and longer fatigue life were observed in hybrid joints that provide a full lateral clamping pressure compared to the adhesive joints. Islam and Tong [24] reported that hybrid steel-glass fibre pre-pegged co-cured single lap joints with stainless steel pins revealed improved static failure strengths of 58% compared to the adhesively bonded joints. The adhesive in the hybrid joint was continually studied to enhance the in single lap joint strength by adding mechanical fasteners. Therefore, the addition of mechanical fasteners of the bolt into bonded joints satisfies the requirements for primary aircraft structures [25]. Pinto et al. studied the effect of hole drilling in aluminium alloy adherends on the strength of single lap joints [14]. The adhesive Araldite was filled in the holes to investigate the stress concentration within and the sharp edges in the holes were located. The study has found that a significant deformation and stress arrest affected around the bolt hole, in which the stress concentration exceeds the cohesive strength.

The selection and stiffness of the adherend material are one of the critical parameters determining the joint strength. In addition, the materials can be vital factors that affect the stress distribution along the overlap area [26, 27]. This includes similar and dissimilar materials of metallic alloys and composite laminates. According to Reis et al. [28], the joint strength was higher with a stiffer adherend for similar adherends subjected to tensile shear loading. Meanwhile, the joint strength in dissimilar adherends was dependent on the strength of the adherend in the same joint configuration. The possibility to join dissimilar materials (composite/metal) by the riveting system was investigated by Fratini and Ruisi [29]. Raju et al. [30] performed three-dimensional finite element model (FEM) analysis for improving load-sharing in single-lap composite hybrid (bolted/bonded) joints. A new design of interference-fit was developed based on the analysis. The interference-fit revealed approximately 10% higher load sharing, with a lower radial stress around the bolt hole. However, the superior new design interference-fits are limited to specific values. The load sharing between the adhesive and bolt was also investigated by Bodjona [31].

In the present study, the effect of different adherend types with combinations of similar and dissimilar AA7075 and GRE composites on the joint strength of single lap joints was investigated. The single-lap joint has been employed by the scientific community owing to its simplicity, as its mechanical properties can be easily determined. The specimens were prepared in three joining configurations: mechanically fastened Huck bolted, adhesively bonded, and hybrid joints (bolted/bonded). The joints were prepared using the Araldite epoxy adhesive and Huck-bolt as a mechanical fastener for joining. The effect of joining technique was evaluated for static and fatigue loading at a constant stress ratio and frequency. Finally, the failure mechanisms in each joint were observed and discussed.

## 2. Methodology

### *2.1. Material selection*

The adherends used in this study were the non-heat treatable aluminium alloy AA7075 and GRE composites. The method used to fabricate the GRE composites specimen was vacuum infusion, as shown in Fig. 1 [31]. The GRE composite plate was fabricated using a [0/90º] woven glass fibre mat with the dimensions of (430 mm x 330 mm x 0.15) mm per layer to achieve an even distribution of the fibres throughout the plates. A releasing agent was applied on top of the glass mould surface for the easy removal of the plates. The Epoxy Amite 100 series resin was mixed with a hardener in the ratio of 3:1 to form the matrix. Afterwards, the woven glass fibres were placed in the desired stacking sequence, and the resin was infused into the lamination plies, as shown in Fig. 2, by a high-vacuum pump (AST 22 model AIRSPEC) under 10 bar pressure [32]. Finally, the specimens were left to cure inside the mould for 12 h at room temperature (25 °C). The selected representative epoxy adhesive was araldite (Huntsman Advanced Materials, Basel, Switzerland). Araldite is a two-part adhesive, with a ratio of 1A:1B by weight. The mechanical properties of AA7075, GRE composites, and the Araldite epoxy adhesive are listed in Table 1.

### *2.2. Joint specimen preparation*

The specimens were prepared in the single-lap joint configuration for similar and dissimilar adherends of AA7075 and GRE composites. Different joining techniques were employed in the study, i.e., mechanically fastened bolted, adhesively bonded and hybrid bolted/bonded joints with ( 160 mm × 40 mm × 3±0.4 mm ) dimensions, as shown in Fig. 3. In order to prepare the specimens, the GRE composites were drill-cut from a solid plate woven (3±0.5 mm thick × 430 mm × 330 mm) into the desired dimensions as mentioned previously. Meanwhile, AA7075 was cut by the supplier (CBM Technology Sdn. Bhd.). Then, for the bonding process, a jig was designed to ensure that the adhesive was equally dispersed along the overlap length of the specimens, as per the procedures of the manufacturer. The precise jig enabled the control of the adherend alignment and adhesive thickness along the overlap length. The overlap length value of 64 mm was calculated from the formulation given in [33]. The thickness of the Araldite epoxy adhesive was set at 0.2 mm. In this experiment, the surface of AA7075 and GRE composites were pre-treated with sandpaper before both sides of the area were cleaned using acetone and wiped off with a microfiber cloth. The purpose was to remove the residual particles that could significantly influence the joint performances and failure

mechanisms. The joint fabrication process is shown in Fig. 4. The bolted and hybrid joints were connected using a pneumatic Huck bolt installer under the air pressure of 90 psi. The fasteners of Huck lockbolt, made of carbon steel were supplied by Arconic Fastening Systems and Rings. The C6L bolt geometry and mechanical properties are shown in Fig. 5 and Table 2, respectively. A total of five replicates were prepared for each joint configuration.

*2.3.Experimental setup*

Tensile testing was performed for mechanically fastened bolted, adhesively bonded and hybrid joint single lap joints using a Shimadzu Universal Testing Machine with a 100 kN load cell. The testing was done at room temperature in accordance with ASTM1002 [34] and ASTM D5868 [35] standards for AA7075 and GRE composites bonding, respectively. At the speed rate of 1 mm/min, five specimens were tested under tension-shear loading until final failure to determine the changes in strength and the behaviour of joints. The peak load and average data were recorded and calculated. The GRE plate was placed on top, while AA7075 was place at the bottom as reported by [16, 36-37].

Fatigue tests were performed using a fatigue test machine with a 100 kN load cell at seven different load amplitudes. The test was conducted in the load control mode with a sinusoidal waveform at a frequency of 5 Hz. The joints were subjected to tension-shear fatigue, with a stress ratio ($R = \sigma min/\sigma max$) of 0.1. The fatigue strength was analysed by drawing S-N curves, and the fatigue fracture surfaces of the tested samples were critically observed. For higher accuracy three replicates were tested at each stress level.

*2.4 Surface morphology of joints*

The fracture surface morphologies associated with the different types of joining techniques were examined using FESEM (NOVA NANOSEM 450). The fractured portions of the samples were cut, and platinum was uniformly coated over the surfaces prior to scanning. The scanned images were obtained at accelerating voltages of 3–5 kV under magnifications of 110× and 2000×.

## 3. Results and discussion

### *3.1. Tensile properties*

The similar-AA7075/AA7075, similar-GRE/GRE, and dissimilar-AA7075/GRE joints were subjected to tensile tests at room temperature (25 °C). The investigations involved different joining techniques: mechanically fastened bolted, adhesively bonded, and hybrid (bonded/bolted) joints to determine the stress-strain behaviour, joint modulus, and typical failure mechanism. The stress-strain curves of the three joint techniques are illustrated in Fig. 6 (a)-(c).

The stress-strain behaviour of similar-AA7075/AA7075 is presented in Fig. 6 (a) for the three joining techniques. This figure shows that mechanically bolted joint reveals a higher failure strength than an adhesively bonded joint (i.e., 44.52 MPa for a mechanically bolted joint, and 37.18 MPa for an adhesively bonded joint). Moreover, the mechanically bolted joint reveals a higher failure strain than the adhesively bonded joint (i.e., 6.41% for the mechanically bolted joint, and 2.96% for an adhesively bonded joint). However, the failure strength of the bonded joint is higher than that of the bolted joint in the case of similar-GRE/GRE interfacial bond adherends as shown in Fig. 6 (b). The lower failure strength observed in the case of bolted joint was due to the thin and relatively flexible GRE composites that also allow the Huck bolt to tilt, increasing the stress concentration at the edge of the hole. A similar observation was reported for the bolted joints of carbon-fibre reinforced plastic adherends in [38]. The Huck bolt joining transfer was evaluated for the largest magnitude of strain, which is related to the failure mechanism of the joint that will be discussed in section 3.3. The similar-GRE/GRE bonded joint yielded linearly elastic behavior, with approximately 91% greater strength than the similar-GRE/GRE bolted joint. The GRE composites deforms as much in the case of a hybrid joint as the Huck bolt supported, after final adhesive bond failure in an adhesively bonded joint.

The performances of dissimilar-AA7075/GRE for the three different joining technique was plotted as stress-strain curves, as shown in Fig. 6 (c). By comparing the maximum tensile strength of the strongest joint of the hybrid with that of the dissimilar-AA7075/GRE, the differences were found to be 83% and 25.9% higher than that of the adhesively bonded joint and the that corresponding to adhesive failure in the hybrid joint, respectively. The mechanically bolted joint registered the lowest stress for dissimilar-AA7075/GRE relative to similar-AA7075/AA7075 and similar-GRE/GE, with reductions of 63.1% and 47.8%, respectively. Based on Fig. 6 (a)-(c), it was observed that the failure stress increase with a

combination of the Araldite epoxy adhesive and Huck bolt in the hybrid joint for each similar and dissimilar adherend connection.

The performances of the hybrid joints, derived from Fig. 6 (a)-(c), are illustrated in Fig. 7 to reveal the stress-strain behaviour of the adhesively bonded joint primarily dominated by the adhesive followed by the Huck bolt as it use in mechanically bolted joint. The joint behaviour was expressed using the stress-strain curve, which was divided into four stages: SI= initial loading, SII= joint split in the adhesive, SIII= post-slip loading of fasteners and SIV= unloading; corresponding to the ultimate tensile strength. Since the hybrid joints comprised a combination of the Araldite epoxy adhesive and Huck bolt, two peak points were observed. The magnitude of the first peak was clarified as the strength of the hybrid joint after initial loading, SI, before the primary failure of the adhesive failed. However, the second peak was observed as the ultimate failure stress including the load of the Huck bolt. Generally, in such cases, the first peak usually has a smaller magnitude than the second peak [19].

The initial loading in SI for the similar-GRE/GRE hybrid joint shows a better strain at failure compared to similar-AA7075/AA7075 and dissimilar-AA7075/GRE. In this stage, the strength of the GRE composites was relatively high in deformation change as it was applied in dissimilar-AA7075/GRE compared to similar-AA7075/AA7075. The joint slip in SII is defined as the primary failure of the Araldite epoxy adhesive as captured in the overlap bond when the adherend slipped relative to the adhesive. However, the hybrid joint was subjected to post-slip loading in SIII that was sustained by the mechanical fasteners of the Huck bolt after the post-adhesive failed. The fracture was observed when ultimate stress reached due to the large applied load. It can be concluded that the high elastic modulus exhibited when the Huck bolt was attached as the joint support for both joining, which bolted and hybrid in second support after adhesive. Besides that, the presence of the mechanical fasteners of the Huck bolt improved the overall strength of the bolted joints by achieving the highest elongation. Indeed, the combination of these two characteristics was found to enhance the performance of hybrid joints, and thus preventing sudden catastrophic failures. The failure loads of the hybrid joints were nearly identical to those of the adhesive joints, and were at least twice as high as those of the mechanical joints.

The responses of the ultimate failure stress and joint modulus for the different types of joining techniques are plotted in Fig. 8 and Fig. 9, which represent the averages with error plots of the obtained results for the five replicates based on the maximum and minimum values, respectively. The deterioration in the mechanical properties was initially found in similar-AA7075/AA7075, similar-GRE/GRE, and dissimilar-AA7075/GRE in the case of

mechanically bolted joints. The decrease was observed for the GRE composites subjected to joining. On the other hand, an increase in strength was observed for the adhesively bonded and hybrid joints for all types of adherend combinations. A loss in strength of the similar-AA7075/AA7075 adhesive bonded joints is suspected due to the weak interfacial interactions between the adherend and the adhesive itself. As mentioned above, the adhesive has a lower surface tension than AA7075, which probably could be affected by UV irradiation or creep under loading.

Based on the design considerations, a high strength during joining was found in the hybrid joints, and the effect of different adherends on mechanical behaviour was an essential factor as the dissimilar AA7075/GRE revealed a more considerable strength. The stress loss gap in overlap bond was filled and strength up by implementing the Huck bolt as it reached a maximum in hybrid strength. From the experimental results carried out, it was found that the mechanically bolted joint is not suitable for joining techniques involving the use of different adherends. This was proved based on the lowest failure strength shown in Fig. 8. To overcome this problem, hybrid joints were introduced and found to be suitable for use when connected to different adherends. This is clearly shown in the bar chart, where the hybrid joints of dissimilar-AA7075/GRE reached the highest strength at failure. The observation presents an interesting finding because this value shows that by using the hybrid joint technique can greatly improve the failure stress of joints involving dissimilar adherend.

Fig. 9 shows the effect of joint configuration on joint modulus for the similar and dissimilar adherends of AA7075 and GRE composites. In both the joining cases, the elastic modulus was constant throughout the elastic region, where the stress was directly proportional to the strain. The experimental values show that the similar-AA7075/AA7075 resulted a higher joint modulus in the case of the hybrid joint compared to those for the bolted and bonded joints, with relative increments of (more than hundred percent; 113% from bolted joint, 16.67% from bonded joint). Furthermore, the joint modulus of similar-GRE/GRE also increased by 0.52, 0.67, and 0.74 GPa for the bolted, bonded, and hybrid joints, respectively. Slightly increases in the joint elastic modulus were observed for dissimilar-AA7075/GRE: 0.62, 0.69, and 0.95 GPa, representing increases of 11.3% and 37.7%, respectively with a respect to bolted and bonded joints. A test summary for each joint in similar and dissimilar adherends is included in Table 3.

*3.2. Fatigue analysis*

The S-N curves denote the maximum stress amplitude plotted against the number of cycles to failure, and are shown in Fig. 10 (a)-(c). The test specimens were evaluated for mechanically fastened, adhesively bonded and hybrid joints with similar and dissimilar adherends of AA7075 and GRE composites. A summary of the fatigue life of each joint involving similar and dissimilar adherends is included in Table 4. Seven different stress levels were used for each joint: 30%, 40%, 50%, 60%, 70%, 80% and 90% of the ultimate tensile load.

Based on Fig. 10 (a) for the mechanically fastened bolted joints, failure was most prolonged cycles for the dissimilar-AA7075/GRE laminates at the reference stress level and amplitude of 30% and 4.9 MPa, respectively. From the observation, crack growth was initially suspected to take place on the AA7075 adherend along the transverse direction near the bolt hole. The equality resulted in 15k cycles that were measured for both similar-AA7075/AA7075 and similar-GRE/GRE joints. However, according to Fu and Mallick [21], the performance of single lap joints SRIM bolted composites prepared by injection moulding were reported to exhibit the most extended fatigue life compared to a hybrid joint subjected to over 2 million cycles. The similar-AA7075/AA7075 achieved the highest stress amplitude compared to similar-GRE/GRE and dissimilar-AA7075/GRE. The S-N curves derived experimentally for the adhesively bonded joint specimens are shown in Fig. 10 (b). The shortest life was recorded for similar-AA7075/AA7075 specimens, which consistently failed after slightly above 200k cycles, followed by the similar-GRE/GRE and dissimilar-AA7075/GRE specimens, which failed between 373k and 700k cycles. According to this observation, none of the joint specimens run out to 1 million cycles at the various stress levels.

The S-N curve of the hybrid joints was plotted, and is shown in Fig. 10 (c) for a combination of similar and dissimilar adherends. According to the curve, the hybrid joint shows the largest and longest fatigue life with over 800k cycles for the dissimilar-AA7075/GRE adherend. It was followed by similar-GRE/GRE and similar-AA7075/AA7075 with 673k and 427k cycles, respectively. More precisely, the presence of Huck bolt fasteners in the hybrid joint aids in arresting the opening of cracks initially, as it is impossible to crack down on the joint once the adhesive failed; this significantly improves fatigue resistance in the early stage. However, in our observation, there is no residual strength for the run out specimen in the present study, as was reported previously by Gordon at lower loads ($\leq$ 30-40% of the static load at failure) for similar carbon fibre composites. The higher resistance to fatigue failure compared to the bonded joints was reflected in the performance of the hybrid joint [38].

Chowdury et al. [20] reported that similarity the hybrid joint configuration performed better than the bonded and mechanically fastened joints in the case of carbon fibre adherend.

*3.3. Failure mechanism*

There are several types of failure mechanisms associated with the joint configurations of the mechanically fastened bolted, adhesively bonded, and hybrid joints, as depicted in Fig. 11. The failures are observe from tensile testing into different joint configuration and types of adherend. A mechanically fastened Huck bolted joint, as illustrated in Fig. 11, shows deformation failure in the bearing mode and net tension. Both the failures were observed in similar-GRE/GRE and dissimilar-AA7075/GRE. It is particularly significant in the single-lap joints with a single bolt, where the load was transferred from one plate to another. From the failure image, it can be observed that the carried load in the similar-AA7075/AA7075 specimens yielding the adherends and rotated the bolt as well thus resulted in both; shear and tension and local bending stress under the head and nut. The adherend yielding in similar-AA7075/AA7075 was detected at the edge of the bolt hole.

The failure mechanism in the adhesively bonded joints can be categorised into adhesive and adherend failures for similar-AA7075/AA7075 and GRE/GRE and dissimilar-AA7075/GRE. The most commonly observed failure mechanism in the bonded joints is the failure at the bondline involving the AA7075 adherend and cohesive failure with fibre tear adherend failure in the GRE composites structures. The adhesive failure in the AA7075 adherend in similar-AA7075/AA7075, and dissimilar-AA7075/GRE contribute to short deformations. Meanwhile, the similar-GRE/GRE joint revealed a long elongation.

Typical failures of the mixed mode and cohesive type were observed as the primary failure mechanism in the hybrid joint of the Araldite epoxy adhesive with similar-AA7075/AA7075 and similar-GRE/GRE, respectively. The hybrid joint of similar-AA7075/AA7075 demonstrates adhesive mixed mode failure and adherend yielding that are correspond to lower joint failure strengths. On the opposite end, the dissimilar-AA7075/GRE demonstrates the highest joint failure strength when cohesive and net tension were detected as the failure mechanism, although that common failure was considered as the sought after failure mode. The phenomenon occurred in the primary failure of adhesive, which indicates excellent bonding between the adherends. For the combination of the Araldite epoxy adhesive and Huck bolt, the hybrid joint carries the load distribution on the specimens, with two failure stages as a failure in adhesive and Huck bolt. It can be concluded that the net-tension, shear-out, and bearing modes

occurred in all the joints for the composites of GRE. This can be attributed to the large elongations of the GRE composites adherend. The elongation, however, generates a large hole in the bearing mode. Thus, the bolt failure mechanism in GRE composites has not been predicted, and is very much depended on the orientation of the fibres of the laminate material.

FESEM was used to examine the surface morphology of the joint configuration of dissimilar-AA7075/GRE under tensile testing, and the corresponding images are shown in Fig. 14 (a)-(d). The adhesive layer remained on the surface of one adherend of the GRE composites as demonstrative samples to determine the failure mode involving fibre/matrix bonding between the adhesive and Huck bolt. The micrograph of the surface, as shown in Fig 12 (a), revealed GRE composites that were bonded to the Araldite epoxy adhesive. In this region, the adhesive was evenly distributed along the overlap length, as it shows no voids, and it is possible to identify the adherend surface even as it is covered with the adhesive. It can thus be inferred that failure was transferred from one adherend to the other. The evidence for the failure mechanism in the GRE composites that rupture along the critical point and experience stock-break failure can be found in the micrograph shown in Fig. 14 (b)-(d). These regions can be found to have experienced shear-out and net-tension at the joint as referred to as secondary failure that occurred in the presence of the Huck bolt. Failure was observed in the GRE composites instead of the AA7075 adherend, as revealed by the fibre carried from implementing failure. The fibre breaks and the fragments remaining on the surface of the adherend are visible, as shown in Fig. 14 (c); representing the bolting region. The resin laminate of the GRE composites was observed after this breaking and detected small voids. Fibre tracks, regions where fibres were pulled away from the matrix, are visible in Fig. 14 (d). The smooth, dark appearance of the back surface here signifies that this is an adhesive layer, indicating that failure in the region occurred in the GRE composites layers.

## 4. Conclusion

The mechanical properties of the different joint configurations of mechanically fastened bolted, adhesively bonded, and hybrid joints were investigated through experimental evaluations. The adherend involved in this study includes AA7075 and GRE composites for combination of similar and dissimilar joining. The mechanical fasteners of the Huck-bolt and Araldite epoxy adhesive were applied for the bolted and bonded joints, respectively. A combination of these two materials was implemented in the hybrid joints. Furthermore, the effects of joining technique, types of adherends and loading rate were investigated in this study. A comparison of the three joint configurations revealed significant differences in the behaviours of the joints involving the adhesive and Huck bolt. This indicates that adhesive and Huck bolt load transfer behaviour essentially functioned independently of each other. The conclusions from this investigation are as follows:

- The hybrid joint with the dissimilar-AA7075/GRE adherend achieved highest ultimate failure strength compared to those of the bolted and bonded single lap joints. The stiffness of the hybrid joint was observed to be four times higher than those of the other joining configurations.
- The effects of the adherend type used in the different joining techniques were identified in terms of the failure mechanism after both static and fatigue loading. From the results obtained, net-tension, shear-out, and bearing failure modes were detected in the GRE composites adherend hybridised with the Huck lock bolt. Meanwhile, the AA7075 surface of the adherend was found to experience mixed mode and adhesive failure.
- The failure modes mainly comprise breakage of fibres, extensive delamination, and matrix cracks in off-axis tows, based on optical observations. Additionally, such observations also reveal the many sites of matrix fall-out (i.e., pieces of the matrix that are missing or loose) and the pull-out fibres. This type of damage indicates failure and degradation of the fibre/matrix interface.
- The fatigue damage mechanisms in the GRE composites are considerably more complicated than those in the AA7075 adhrend, since they usually involve different combinations of the damage modes.

**Acknowledgements**

The authors would like to acknowledge all personnel involve in the research. The authors also would like to thank the Ministry of High Education (MOHE), Malaysia for providing financial assistance through the Fundamental Research Grant Scheme (FRGS-MRSA 2018).

**References**

[1] Miller W. Recent development in aluminium alloys for the automotive industry. Mater Sci Eng A 2000;280:37-49.

[2] Lambiase F, Durante M. Mechanical behaviour of punched holes produced on thin glass fibre reinforced plastic laminates. Compos Struct 2017;173:25-34.

[3] Lambiase F, Genna S. Laser-assisted direct joining of AISI304 stainless steel with polycarbonate sheets: thermalnalysis, mechanical characterization, and bonds morphology. Opt Laser Technol 2017;88:205-214.

[4] Lambiase F,Genna S, Leone C, Paoletti A. Laser-assisted direct joining of carbon fibre reinforced plastic with thermosetting matrix to polycarbonate sheets. Opt Laser Technol 2017;94:45-58.

[5] Li Y, Yan Y, Zhang T, Liang Z. Experimental study of adhesively bonded CFRP joints subjected to tensile loads. Int J Adhes Adhes 2015;57:95-104.

[6] Stuparu FA, Apostol DA, Constantinescu DM, Picu CR, Sandu M, Sorohan S. Local evaluation of adhesive failure in similar and dissimilar single-lap joints. Eng Fract Mech 2017;183:39-52.

[7] Arnautov A, Nasibullins A, Gribniak V, Blumbergs I, Hauka M. Experimental characterization of the properties of double-lap needled and hybrid joints of carbon/epoxy composites. Materials (Basel) 2015;8,11:7578-7586.

[8] Chuang WY, Tsai JL. Investigating the performances of stepwise patched double lap joint. Int J Adhes Adhes 2013;42:44-50.

[9] Liu M, Dawood M. Reliability analysis of adhesively bonded CFRP-to-steel double lap shear joint with thin outer adherends. Constr Build Mater 2017;141:52-63.

[10] Adin H. The effect of angle on the strain of scarf lap joints subjected to tensile loads. Appl Math Model 2012;36:2858-2867.

[11] Adin H. The investigation of the effect of angle on the failure load and strength of scarf lap joints. Int J Mech Sci 2012;61:24-31.

[12] Lee HK, Pyo SH, Kim BR. On joint strengths, peel stresses and failure modes in adhesively bonded double-strap and supported single-lap GFRP joints. Compos Struct 2009;87:44-54.

[13] Sato C. Dynamic stress responses at the edges of adhesive layers in lap strap joints of half-infinite length subjected to impact loads. Int J Adhes Adhes 2009;29:670-677.

[14] Pinto AMG, Campilho RDSG, Mendes IR, Aires SM, Baptista APM. Effect of hole

drilling at the overlap on the strength of single-lap joints. Int J Adhes Adhes 2011;31:380-387.

[15] Chowdury NM, Chiu WK, Wang J, Chang P. Experimental and finite element studies of bolted, bonded and hybrid step lap joints of thick carbon fibre/epoxy panels used in aircraft structures. Compos Part B Eng 2016;100:68-77.

[16] Sugita Y, Winkelmann C, Saponara VL. Environmental and chemical degradation of carbon/epoxy lap joints for aerospace applications, and effect on their mechanical performance. Compos Sci Technol 2010;70:829-839.

[17] Park YB, Song MG, Kim JJ, Kweon JH, Choi JH. Strength of carbon/epoxy composite single-lap bonded joints in various environmental conditions. Compos Struct 2010.

[18] Lu Y, Broughton J, Winfield P. A review of innovations in disbanding techniques for repair and recycling of automotive vehicles. Int J Adhes Adhes 2014;50:119-127.

[19] Lee YH, Lim DW, Choi JH, Kweon JH, Yoon MK. Failure load evaluation and prediction of hybrid composite double lap joints. Compos Struct 2010;92:2916-2926.

[20] Chowdury N, Chiu WK, Wang J, Chang P. Static and fatigue testing thin riveted, bonded and hybrid carbon fiber double lap joints used in aircraft structures. Compos Struct 2015;121:315-323.

[21] Fu M, Mallick PK. Fatigue of hybrid (adhesive/bolted) joints in SRIM composites. Int J Adhes Adhes 2001;21:145-149.

[22] Sadowski T, Golewski P, Raczkowska EZ. Damage and failure processes of hybrid joints: Adhesive bonded aluminium plates reinforced by rivets. Comput Mater Sci 2011;50:1256-1262.

[23] Islam MS, Tong L. Influence of pinning on static strength of co-cured metal-GFRP hybrid single lap joints. Compos Part A Appl Sci Manuf 2016;84:196-208.

[24] Lopez-cruz P, Laliberte J, Lessard L. Investigation of bolted/bonded composite joint behaviour using design of experiments. Compos Struct 2017;170:192-201.

[25] Nguyen ATT, Brandt M, Feih S,Orifici AC. Pin pull-out behaviour for hybrid metal-composite joints with integrated reinforcements. Compos Struct 2016;155:160-172.

[26] Afendi M, Teramoto T, Bin H, Yh AL. Strength prediction of epoxy adhesively bonded scarf joints of dissimilar adherends. Int J Adhes Adhes 2011;31:402-411.

[27] Reis PNB, Ferreira JAM, Antunes F, Al A. Effect of adherend's rigidity on the shear strength of single lap adhesive joints. Int J Adhes Adhes 2011;31:193-201.

[28] Fratini L, Ruisi VF. Self-piercing riveting for aluminium alloys-composites hybrid joints. Int J Adv Manuf Technol 2009;43:61-66.

[29] Raju KP, Bodjona K, Lim GH, Lessard L. Improving load sharing in hybrid bonded/bolted composite joints using an interference-fit bolt. Compos Struct 2016;149:329-338.

[30] Bodjona K, Raju K, Lim GH, Lessard L. Load sharing in single-lap bonded/bolted composite joints. Part 1:Model development and validation. Compos Struct 2015;129:268-275.

[31] Cucinotta F, Guglielmino, Sfravara F. Life cycle assessment in yacht industry:Acase study of comparison between hand lay-up and vacuum infusion. J Clean Prod 2017;142:3822-3833.

[32] Humberto J, Almeida S, Luiz H, Junior O, Campos S. Study of hybrid interlaminate curaua/glass compoistes 2012;42:111-117.

[33] Majid M, Afendi M, Liah WW, Hafizan K. Strength of composites hybrid joint. ARPN J Eng Appl Sci 2016;11:216-221.

[34] ASTM D1002. Standard Test Method for Apparent Shear Strength of Single-Lap-Joint Adhesively Bonded Metal Specimens by Tension Loading (Metal-to-Metal), 2010.

[35] ASTM D5868. Standard Test Method for Lap Shear Adhesion for Fiber Reinfoced Plastic (FRP) Bonding, 2014.

[36] Settineri L, Atzeni E, Ippolito R. Self-piercing riveting metal-polymer joints. Int J Mater Form 2010;3:995-998.

[37] Fiore V, Alagna F, Bella G, Valenza A. On the mechanical behaviour of BFRP to aluminium AA6086 mixed joints. Compos Part B Eng 2013;48:79-87.

[38] Kelly G. Quasi-static strength and fatigue life of hybrid (bonded/bolted) composite single-lap joints. Compos Stuct 2006;72:119-129.

[39] Kumar AA, Sundaram R. Cure cycle optimization for the resin infusion technique using carbon nanotubes additives. Carbon N Y 2016;96:1043-1052.

**Figures Captions**

**Fig. 1.** Schematic diagram of the vacuum infusion process.

**Fig. 2.** Vacuum infusion process: (a) materials set up, (b) resin flow, and (c) the vacuum infusion technique.

**Fig. 3.** Typical joining methods for (a) a mechanically fastened bolted joint (b) an adhesively bonded joint, and (c) a hybrid joint (bolted/bonded).

**Fig. 4.** Preparation of single lap joints specimens: (a) an illustration of joint manufacturing, photographs illustrating the (b) application of the Araldite epoxy adhesive on both bonded and hybrid joints, and (c) Huck bolt installation of the hybrid joints.

**Fig. 5.** Dimensions of Huck Lockbolt C6L.

**Fig. 6.** Stress-strain curves of the different joint configurations: (a) similar-AA7075/AA7075, (b) similar-GRE/GRE, and (c) dissimilar-AA7075/GRE.

**Fig. 7**. Plot revealing the tensile stress behaviour for the different stage of the three hybrid joints: SI= initial loading, SII= joint split in the adhesive, SIII= post-slip loading of fasteners, and SIV= unloading; at ultimate failure.

**Fig. 8**. Ultimate failure stresses for the different joining techniques.

**Fig. 9.** Joint elastic modulus for the different joining techniques.

**Fig. 10**. Stress-lifetime (S-N) diagrams for similar-AA7075/AA7075, similar-GRE/GRE, and dissimilar-AA7075/GRE adherends: (a) bolted joints (b) bonded joints (c) hybrid joints.

**Fig. 11.** Types of failure mechanism for bolted, bonded, and hybrid joint configurations.

**Fig. 12**. FESEM images displaying the fractured surfaces of the dissimilar-AA7075/GRE hybrid joint under tensile tests: (a) surface of the GRE composites, (b) fracture of the GRE composites at the edge of the hole, (c) fracture of the GRE composites at the bolting contact surface, and (d) fracture of the GRE composites at the edge of the hole.

## List of Tables

**Table 1**. Material properties of the adhesive and adherends.

| Material | Ultimate Tensile Strength [MPa] | Yield Stress [MPa] | Elastic Modulus [GPa] | Poisson's ratio v |
|---|---|---|---|---|
| **AA7075** | 220 | 95 | 70.0 | 0.33 |
| **GRE composite** | 215 | 79 | 5.6 | 0.22 |
| **Araldite epoxy adhesive [36]** | 23~24 | 21 | 1.4 | 0.38 |

**Table 2**. Huck Lockbolt C6L properties.

| | Shear | Clamp | Tesile | Grip range | Series no. |
|---|---|---|---|---|---|
| **Huck C6L LockBolt** | 1725 (2430) | 1025 (1200) | 1400 (2200) | 8 – 11.1 (mm) | C6LB-R8-6G |
| **Collar** | - | - | - | - | 2LC-R8G |

**Table 3**. Tensile properties of mechanically fastened bolted, adhesively bonded, and hybrid joints.

| Joint configuration | Types of combination | Number of specimens | Average peak load (kN) | Ultimate tensile stress (MPa) | Elastic modulus (GPa) |
|---|---|---|---|---|---|
| **Mechanically fastened bolted** | Similar-AA7075/AA7075 | 5 | 12.47±0.74 | 44.52±2.58 | 0.69 |
| | Similar-GRE/GRE | 5 | 8.81±0.63 | 31.45±2.21 | 0.52 |
| | Dissimilar-AA7075/GRE | 5 | 4.60±0.65 | 16.43±2.27 | 0.62 |
| **Adhesively bonded** | Similar-AA7075/AA7075 | 5 | 10.41±0.44 | 37.18±1.54 | 1.26 |
| | Similar-GRE/GRE | 5 | 14.08±0.65 | 43.16±2.25 | 0.67 |
| | Dissimilar-AA7075/GRE | 5 | 13.50±0.61 | 48.21±2.12 | 0.69 |
| **Hybrid** | Similar-AA7075/AA7075 | 5 | 12.77±0.51 | 45.60±1.78 | 1.47 |
| | Similar-GRE/GRE | 5 | 21.37±0.53 | 76.31±1.84 | 0.74 |
| | Dissimilar-AA7075/GRE | 5 | 24.69±0.61 | 88.19±2.11 | 0.95 |

**Table 4.** Tensile properties of mechanically fastened bolted, adhesively bonded, and hybrid joints

| Joint configuration | Joint materials | No. of cycles to failure at stress level with max. fatigue load (Note: Min. fatigue load/ max. fatigue load = 0.1) x $10^3$ | | | | | | |
|---|---|---|---|---|---|---|---|---|
| | | 30% | 40% | 50% | 60% | 70% | 80% | 90% |
| **Mechanically fastened bolted** | Similar-AA7075/AA7075 | 14.9 | 8.9 | 8.7 | 4 | 3.5 | 2 | 1.1 |
| | Similar-GRE/GRE | 15.1 | 8 | 6.5 | 3.8 | 2 | 1 | 0.6 |
| | Dissimilar-AA7075/GRE | 158 | 19.3 | 15 | 12 | 5 | 3.3 | 0.8 |
| **Adhesively bonded** | Similar-AA7075/AA7075 | 201.2 | 14.3 | 1.7 | 1.1 | 0.6 | 0.4 | 0.09 |
| | Similar-GRE/GRE | 373 | 193 | 31 | 17.9 | 2 | 0.8 | 0.1 |
| | Dissimilar-AA7075/GRE | 700 | 650 | 48 | 39 | 28 | 19 | 2 |
| **Hybrid** | Similar-AA7075/AA7075 | 427 | 381 | 299.9 | 220 | 32 | 15 | 1.2 |
| | Similar-GRE/GRE | 673 | 485 | 41 | 37.8 | 46 | 15.8 | 5 |
| | Dissimilar-AA7075/GRE | 800 | 720 | 550 | 321 | 50 | 7 | 3 |

**List of Figures**

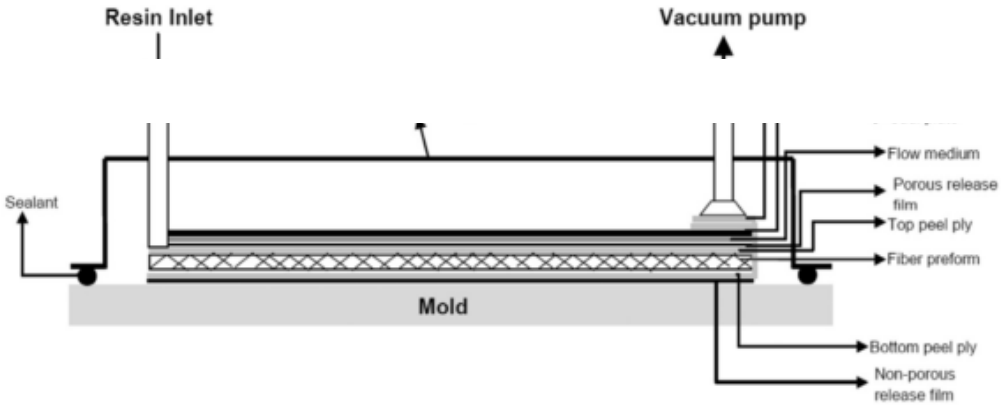


**Fig. 1**. Schematic diagram of the vacuum infusion process [39].

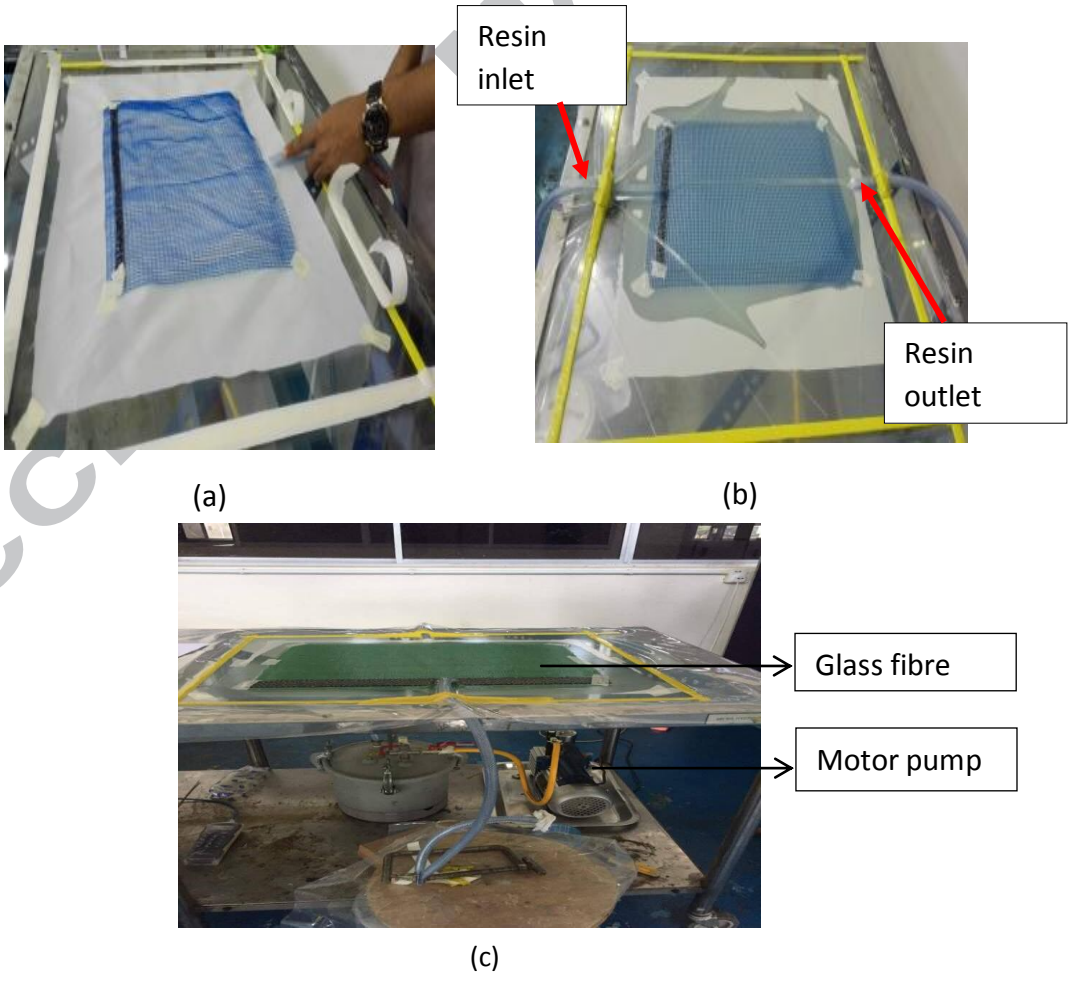


**Fig. 2.** Vacuum infusion process: (a) materials set up, (b) resin flow, and (c) the vacuum infusion technique.

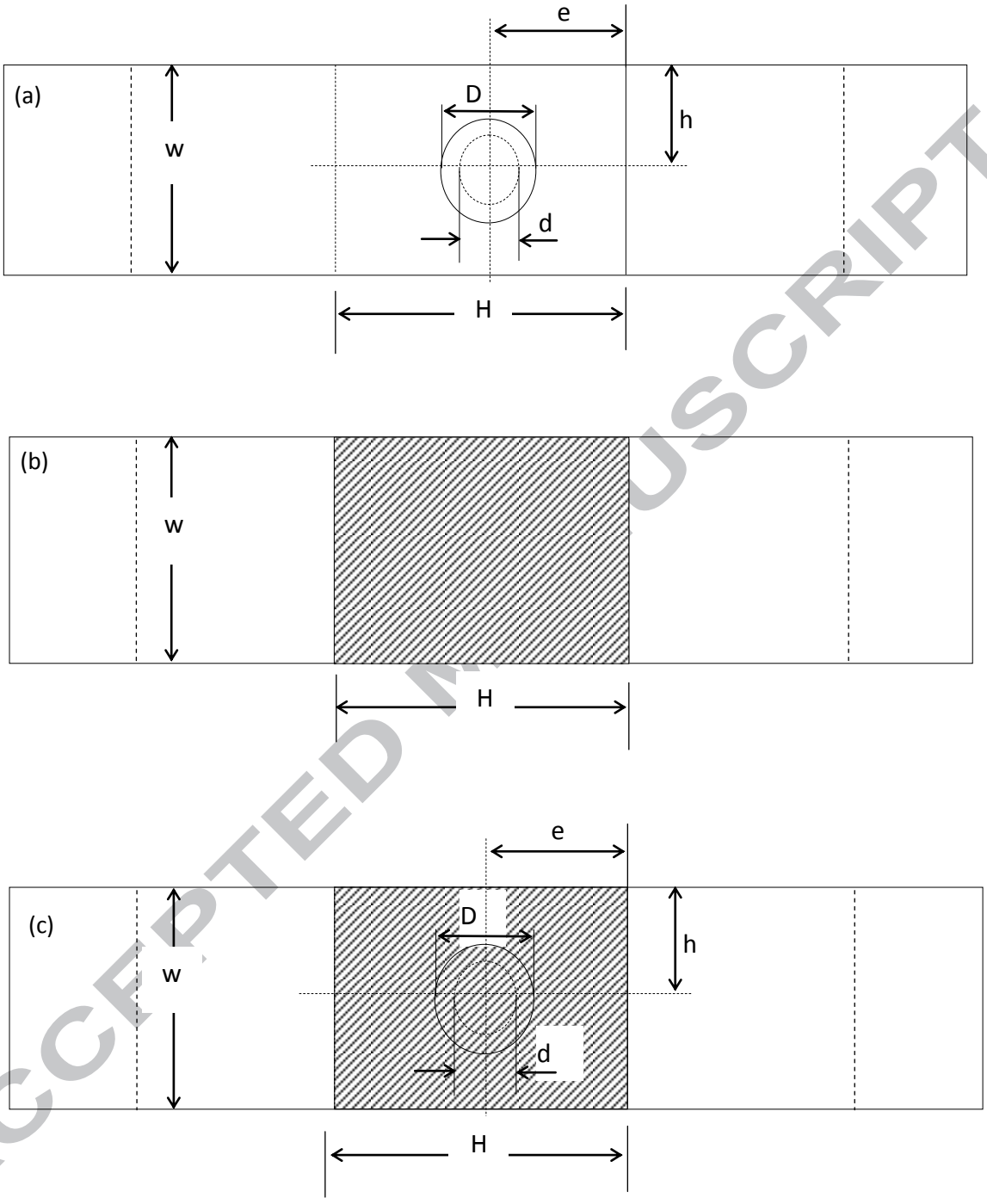


* Single lap joint geometries for bolted, bonded and hybrid with dimension of : L = length 160 mm, w = width 40 mm, H = overlap length, d = bolt hole diameter 6.35 mm.

**Fig. 3.** Typical joining methods for (a) a mechanically fastened and bolted joint, (b) an adhesively bonded joint, and (c) a hybrid joint (bolted/bonded).

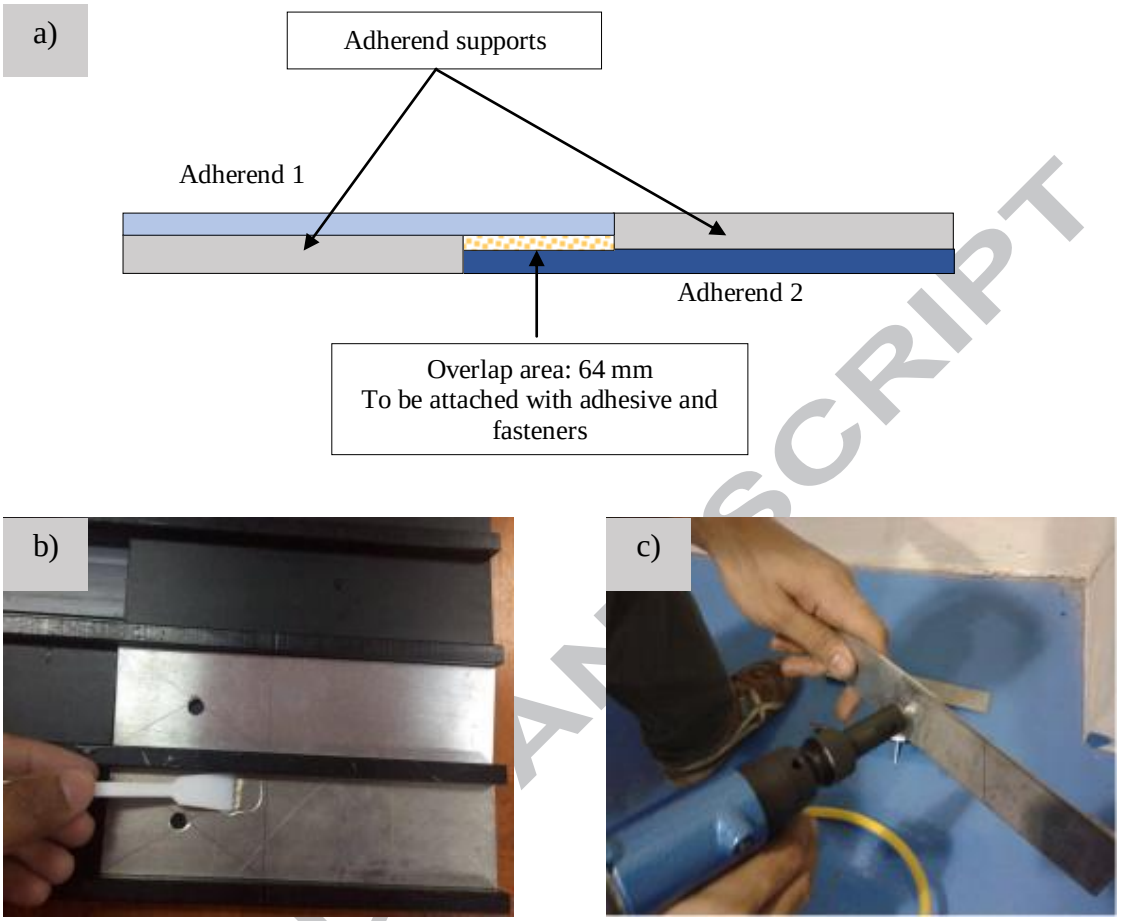


**Fig. 4.** Preparation of single lap joint specimens: a) an illustration of joint fabrication, photographs illustrating the b) application of the araldite epoxy adhesive on both bonded and hybrid joints, and c) Huck bolt installation of the hybrid joints.

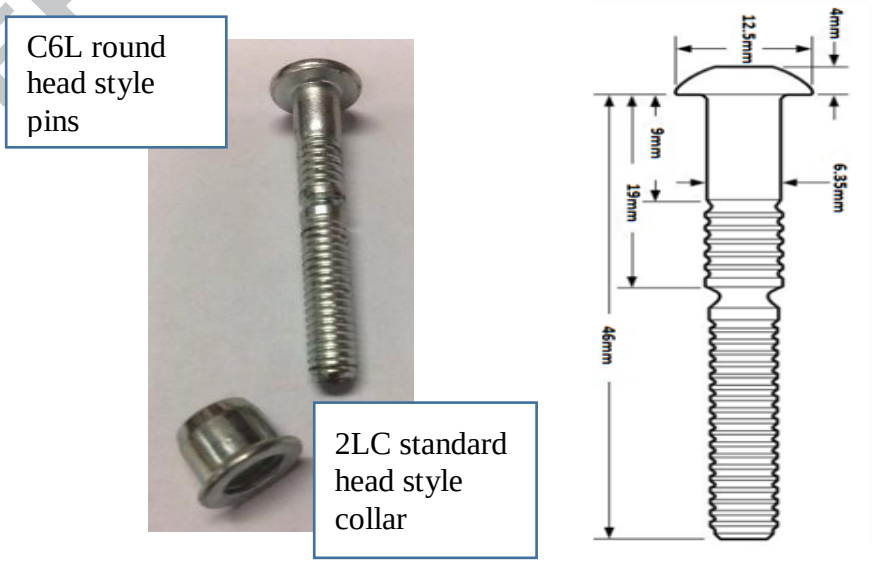


**Fig. 5.** Dimensions of Huck Lockbolt C6L.

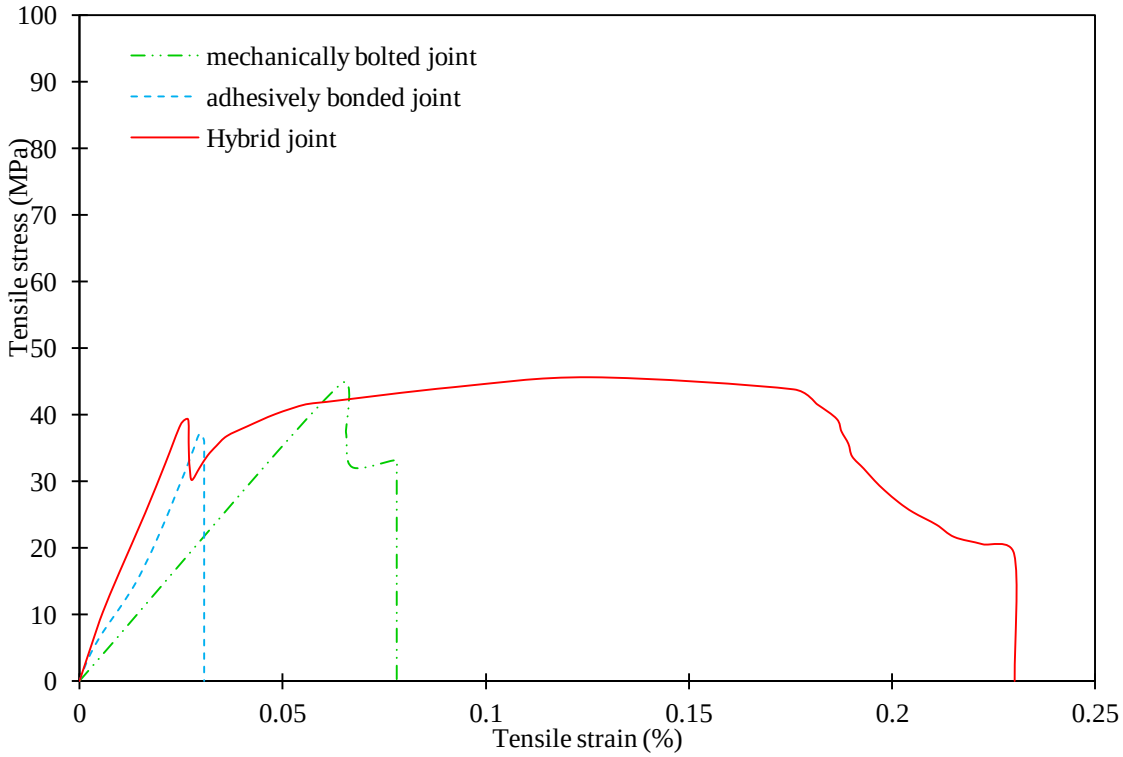


(a)

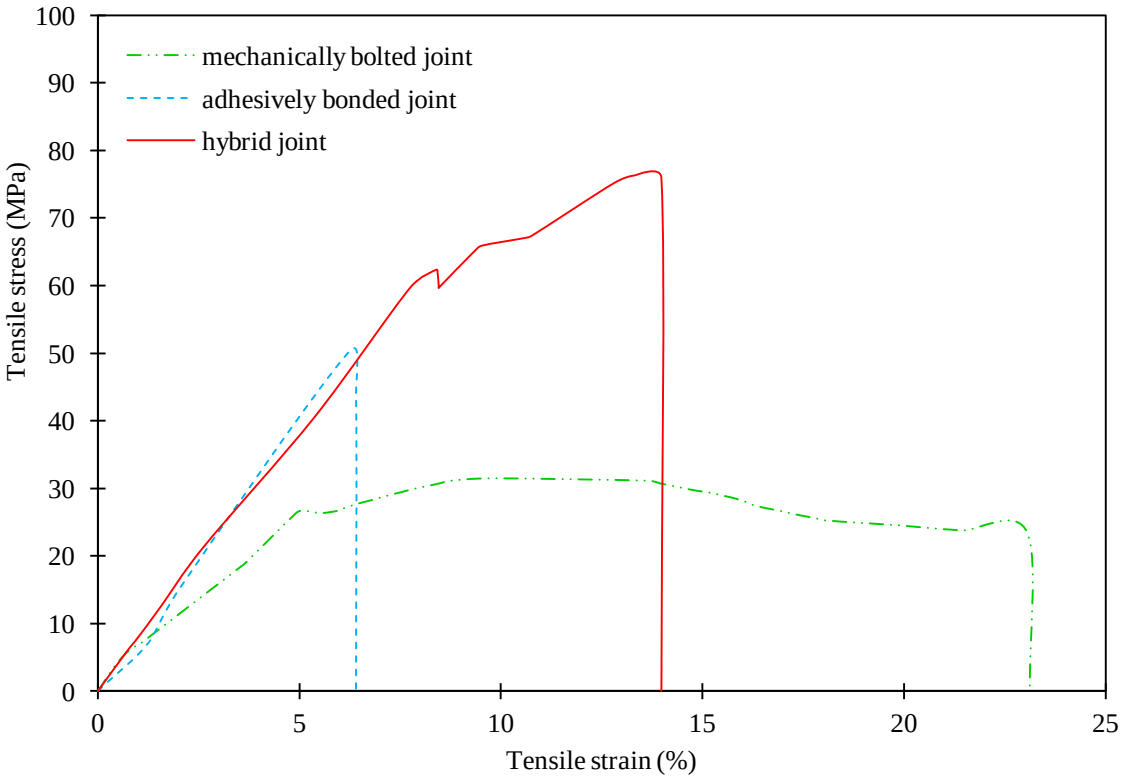


(b)

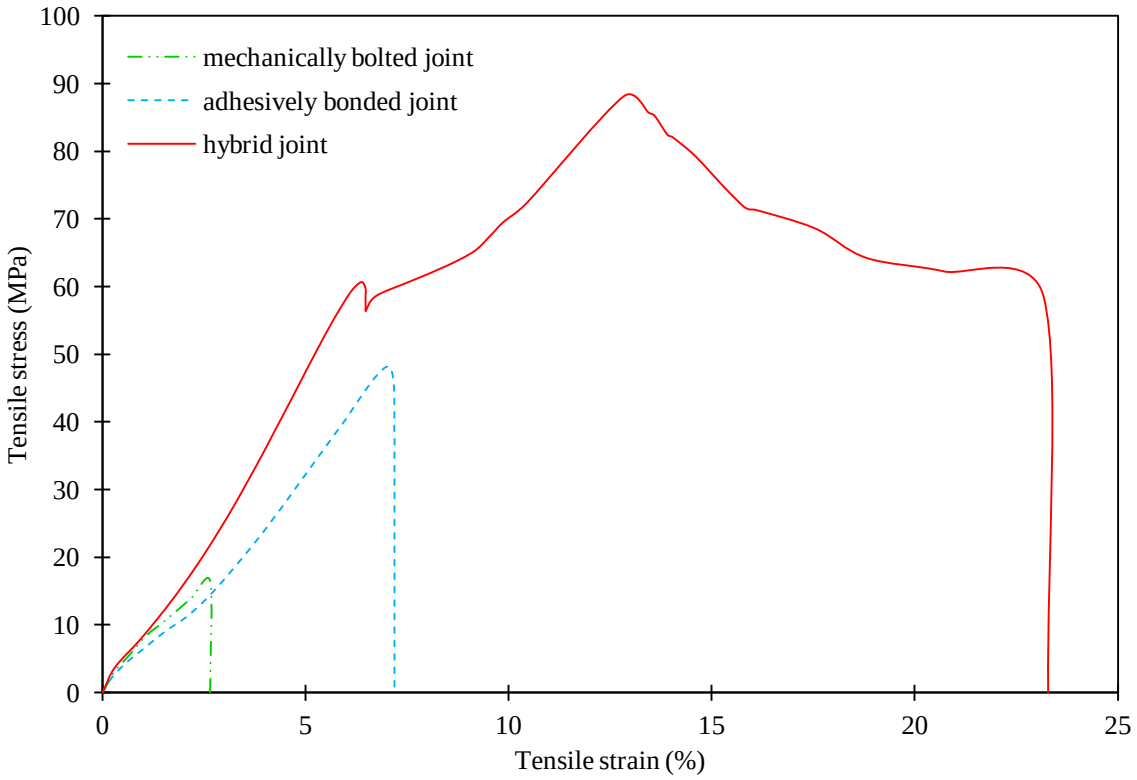


(c)

**Fig. 6.** Stress-strain curves of the different joint configurations: (a) similar-AA7075/AA7075, (b) similar-GRE/GRE, and (c) dissimilar-AA7075/GRE.

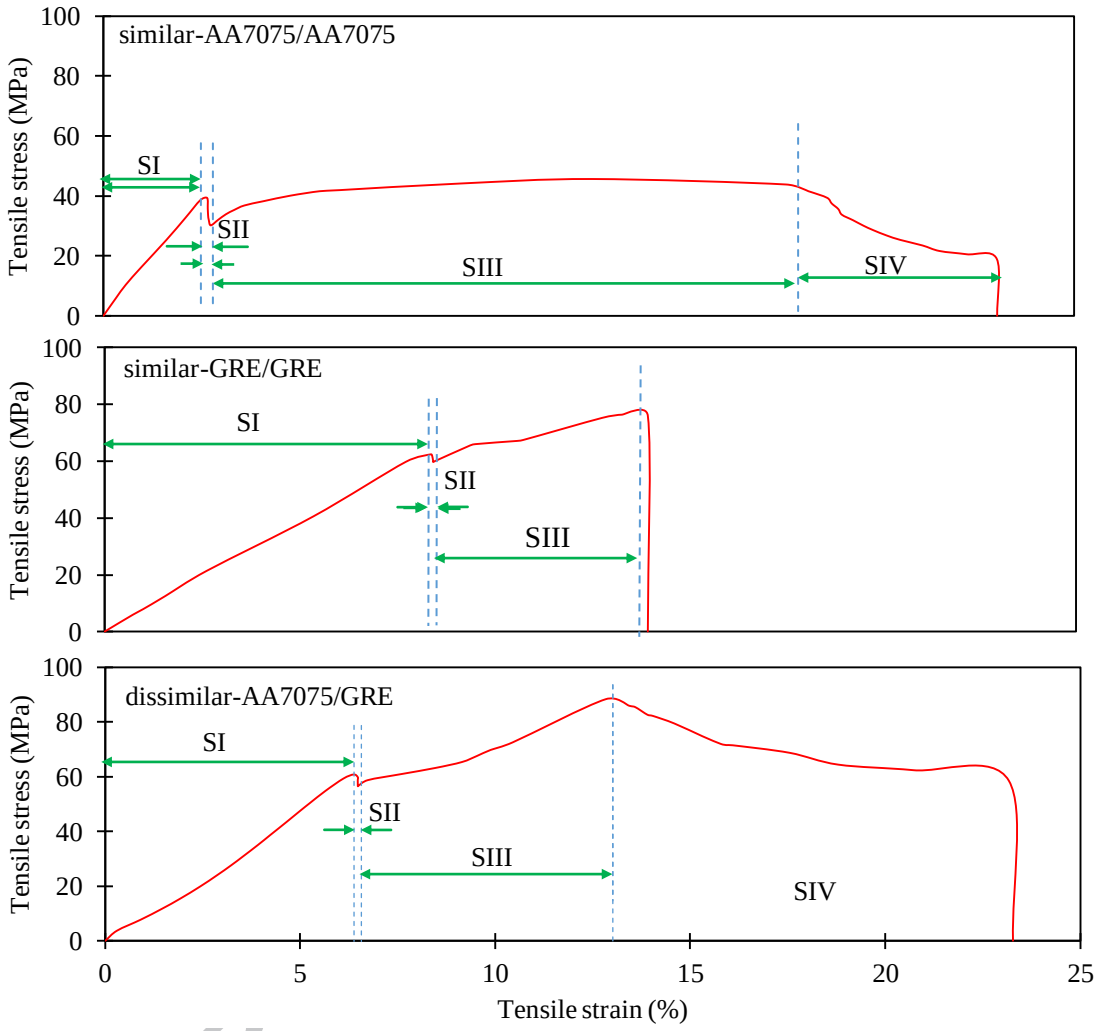


**Fig. 7**. Plots revealing the tensile stress behaviour for the different stages of the three hybrid joints: SI= initial loading, SII= joint split in the adhesive, SIII= post-slip loading of fasteners, and SIV= unloading; at ultimate failure.

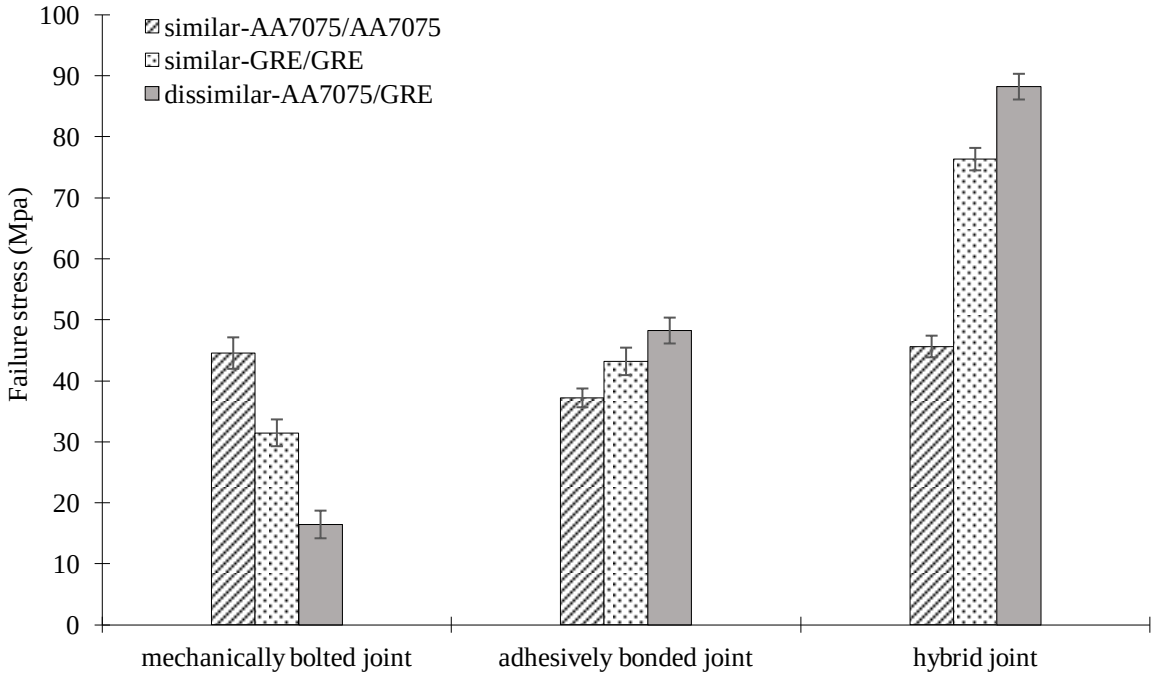


**Fig. 8.** Ultimate failure stresses for the different joining techniques.

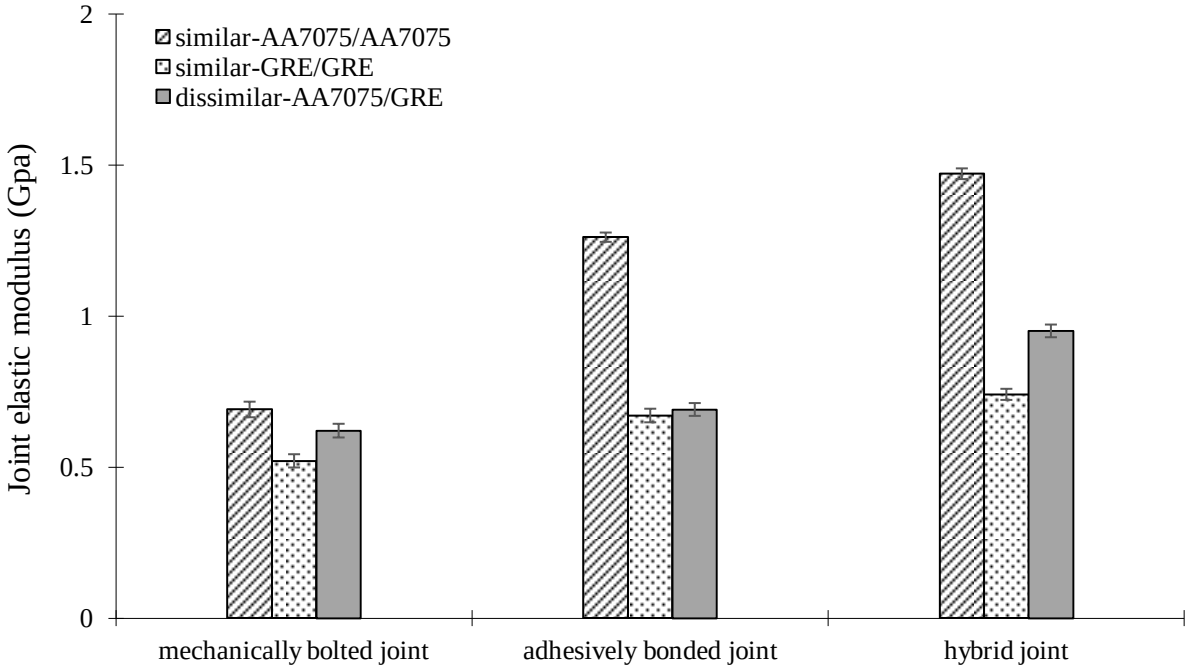


**Fig. 9.** Joint elastic modulus for the different joining techniques

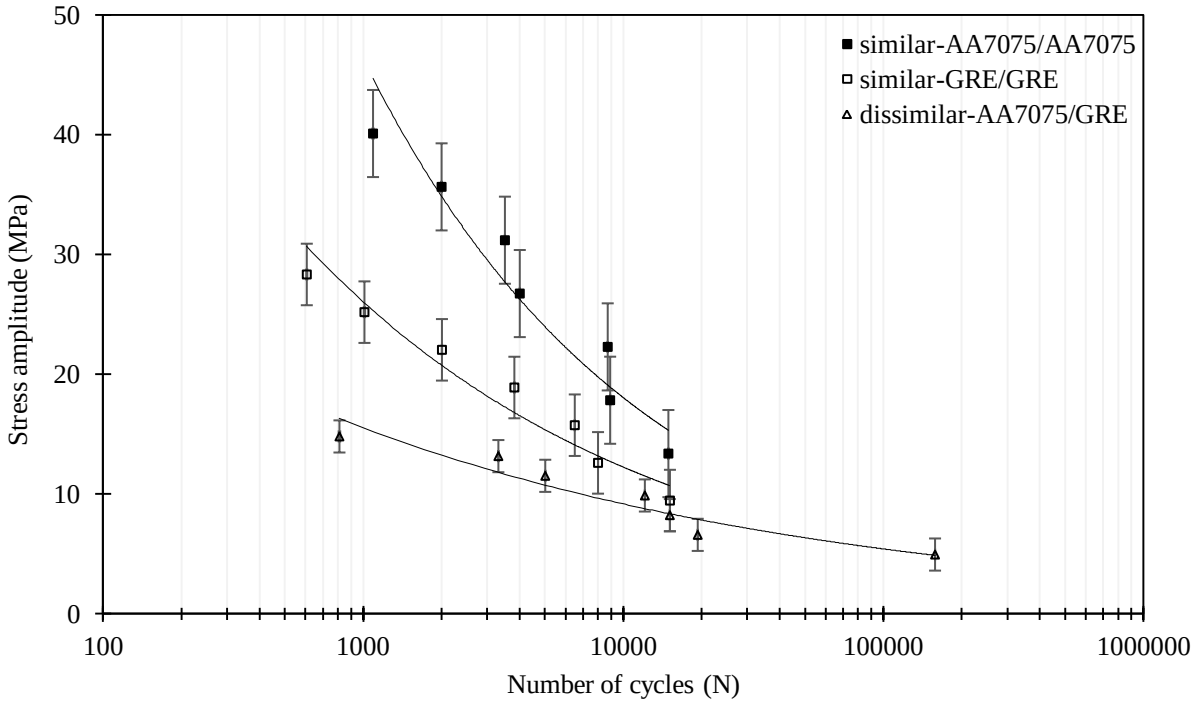


(a)

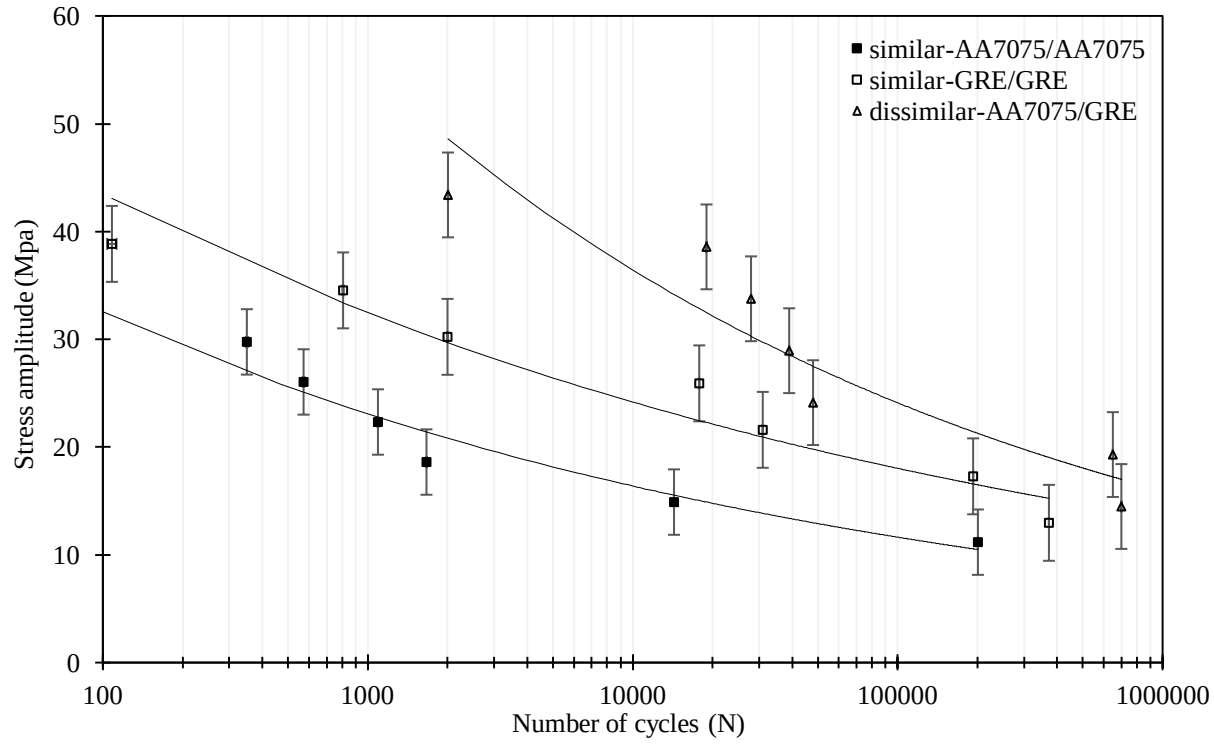


(b)

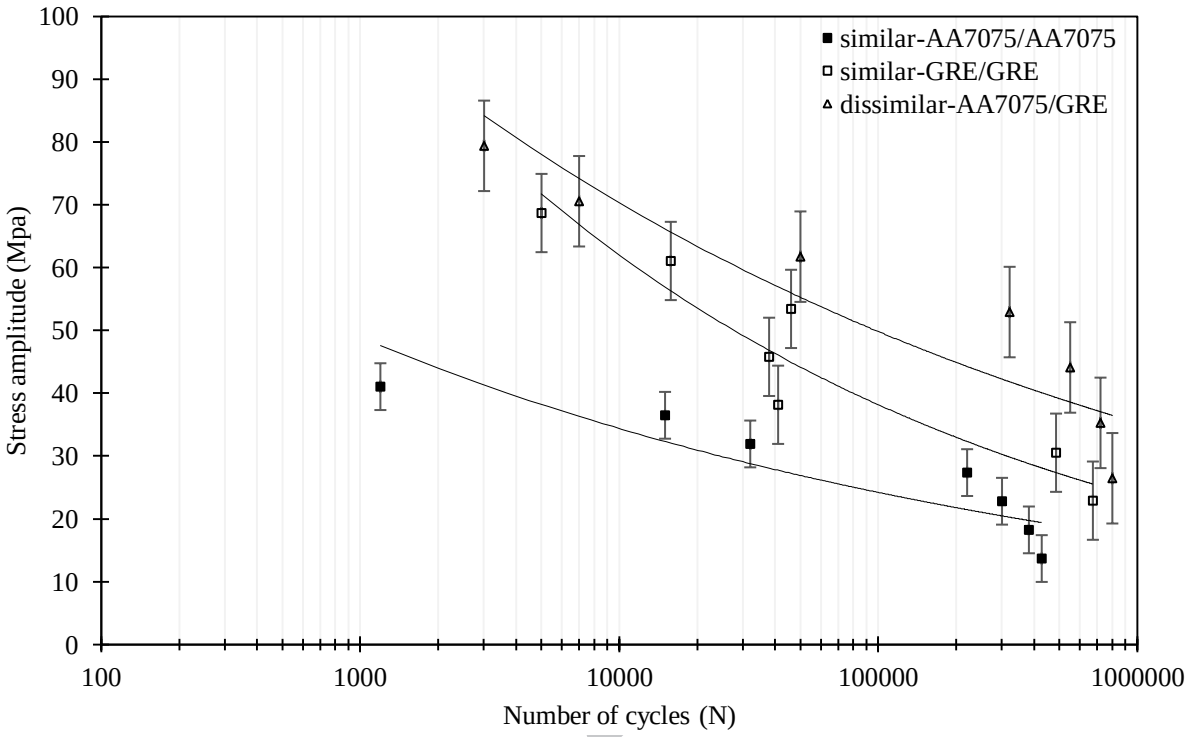


**Fig. 10.** Stress-lifetime (S-N) diagrams for SM-AA7075, SM-GRE, and DS-AA7075/GRE materials: (a) bolted joints, (b) bonded joints, and (c) hybrid joints.

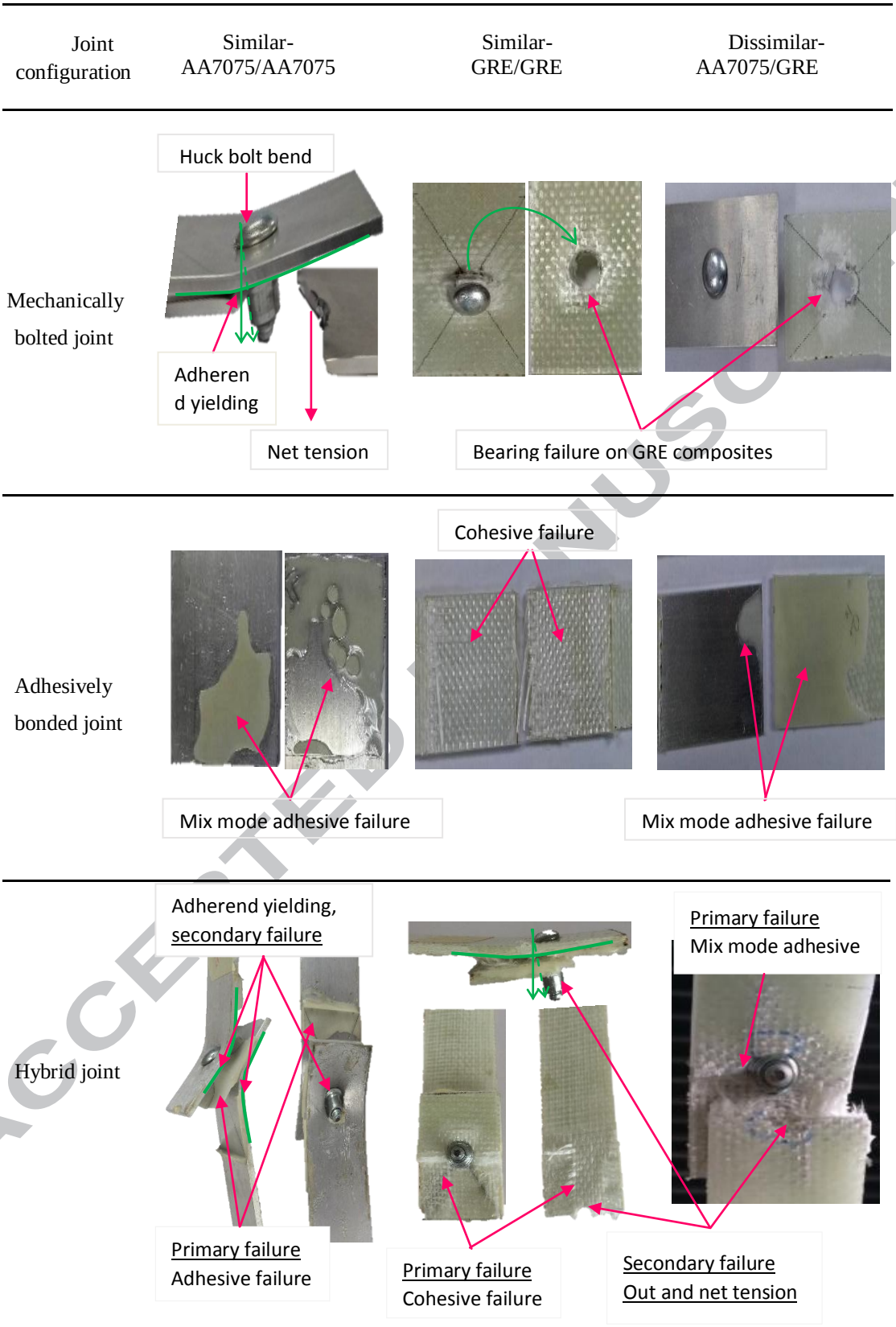


**Fig. 11.** Types of failure mechanisms for bolted, bonded, and hybrid joint configurations.

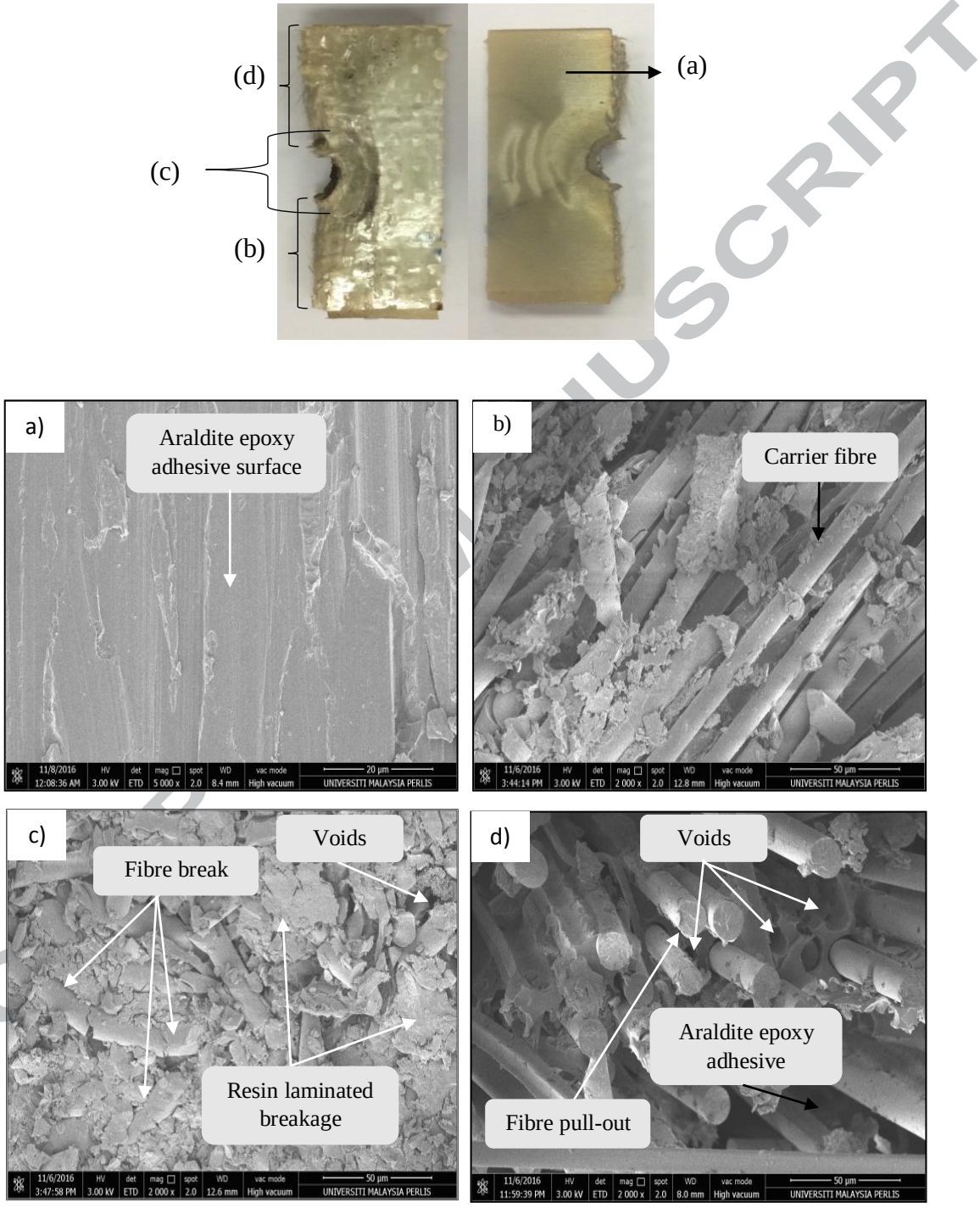


**Fig. 12.** FESEM images displaying the fractured surfaces of the dissimilar-AA7075/GRE hybrid joint under tensile tests: (a) surface of the GRE composites, (b) fracture of the GRE composites at the edge of the hole, (c) fracture of the GRE composites at the bolting contact surface, and (d) fracture of the GRE composites at the edge of the hole.